Int. J. Heat Mass Transfer. Vol. 25, No. 5, pp. 615–624, 1982
Printed in Great Britain

0017-9310/82/050615-10 $03.00/0
Pergamon Press Ltd.

TURBULENCE MEASUREMENTS AND MASS TRANSFER IN FULLY DEVELOPED FLOW IN A TRIANGULAR DUCT WITH A NARROW APEX ANGLE

HIROMOTO USUI, YUJI SANO and HIROMICHI FUKUMA
Department of Chemical Engineering, Yamaguchi University,
Ube 755, Japan

(*Received* 8 *July* 1981)

Abstract—The electrochemical method is applied to the mass transfer measurements in a fully developed turbulent flow in an Isosceles triangular duct with a narrow apex angle. The analysis of the measured fluctuating mass transfer coefficient on a point electrode results in the distribution of turbulent intensity and space correlation coefficient on the side wall of a triangle. In the laminar or transitional region near the apex, a remarkable change in turbulent intensity and space correlation is detected. In addition, even at the fully turbulent region near the base of a triangle, the turbulent characteristics very near the side wall are considerably changed from those of a turbulent round tube flow at the same Reynolds number. The decrease in overall mass transfer coefficient in a triangular duct is qualitatively explained by the change of wall turbulence structure.

NOMENCLATURE

- a, radius of point electrode [m];
- D, mass diffusivity [m^2/s];
- d_h, hydraulic diameter [m];
- f, friction factor;
- K, local mass transfer coefficient [m/s];
- $\bar{K}$, overall mass transfer coefficient [m/s];
- $\bar{k}$, time averaged mass transfer coefficient on a point electrode [m/s];
- k', fluctuating component of mass transfer coefficient on a point electrode [m/s];
- k'_0, measured fluctuating mass transfer coefficient on a point electrode [m/s];
- L, length of the side wall of an isosceles triangle [m];
- Re, $\equiv d_h \bar{U}/\nu$, Reynolds number;
- R_t, Eulerian time correlation coefficient defined by equation (7);
- R_z, lateral space correlation coefficient defined by equation (1);
- $R_{x,t}$, space and time correlation coefficient defined by equation (6);
- Sc, $\equiv \nu/D$, Schmidt number;
- $\overline{Sh}$, $\equiv \bar{K}\, d_h/D$, overall Sherwood number;
- Sh, $\equiv K\, d_h/D$, local Sherwood number;
- $\bar{s}_x$, time averaged velocity gradient on a point electrode [s^{-1}];
- s'_x, fluctuating component of velocity gradient at the wall [s^{-1}];
- t, time [s];
- Δt, delay time [s];
- $\bar{U}$, averaged velocity over the cross section of an isosceles triangular duct [m/s];
- U_c, convective velocity of large eddy near the wall [m/s];
- $\bar{u}$, local mean velocity [m/s];
- u', fluctuating velocity in the longitudinal direction [m/s];
- u^*, local wall shear velocity [m/s];
- x, distance in the longitudinal direction [m];
- y, distance from the wall [m];
- z, distance in the lateral direction [m];
- Δz, distance between the two electrodes [m].

Greek symbols

- θ, apex angle of an isosceles triangle [degrees];
- Λ_x, integral scale of the longitudinal space correlation coefficient [m];
- Λ_z, integral scale of the lateral space correlation coefficient [m];
- ν, kinematic viscosity [m^2/s];
- ρ, density [kg/m^3];
- τ, local wall shear stress [N/m^2];
- $\bar{\tau}$, averaged wall shear stress [N/m^2];
- τ_E, integral scale of Eulerian time correlation coefficient [s].

Superscript

- $+$, non-dimensionalized by wall parameters.

1. INTRODUCTION

BECAUSE of wide technical application, especially in the design of compact heat exchanger, turbulent flow and heat transfer in ducts of non-circular cross-section have been studied extensively in the past. Among the various kinds of non-circular cross-sections, an Isosceles triangular duct with a narrow apex angle has been widely investigated since Eckert and Irvine [1] pointed out that a significant laminar region existed near the apex of a triangular duct while the remainder of the flow was turbulent. Such a flow condition proposes a typical characteristic of flow and heat transfer in a non-circular duct heat exchanger.

The coexistence of laminar and turbulent flow regions in a triangular duct was discussed by Hanks and Brooks [2] and Bandopadhayay and Hinwood [3]. Bandopadhayay and Hinwood confirmed that a significant laminar layer existed in the apex region which seemed to be formed by interaction of the boundary layers on the side walls of the duct. Eckert and Irvine [4] applied Deissler and Taylor's analytical method [5] to an Isosceles triangular duct with a narrow apex angle (11.5°) for comparison with their experimental results. They found that the measured Nusselt number was much lower (around 50% lower) than that obtained for a circular tube flow. The decrease in the heat transfer coefficient was not explained by the analytical prediction. Recently Kokorev *et al.* [6] solved a hydraulic and heat transfer problem in the same geometry. Although they employed a crude assumption on the eddy diffusivity of momentum, their integral method showed a considerable improvement in the prediction of averaged heat transfer coefficient.

Although many investigators have been studying triangular duct flow, turbulent structure in a triangular duct is not clearly understood and the reason for the decrease in averaged heat transfer coefficient is not fully explained. Thus, in this investigation, the electrochemical method was applied to the turbulent flow in a triangular duct to obtain the overall and local mass transfer coefficients. Also the time averaged and fluctuating wall shear stress were measured. The change of turbulent characteristics along the side wall is discussed to give a clear view of the turbulent structure in a triangular duct.

2. EXPERIMENTAL APPARATUS AND PROCEDURE

An isosceles triangular duct with nickel electrodes provided the test section of mass transfer experiments. This test section was fitted to a recirculating flow loop comprising a mixing box, storage tank, centrifugal pump, flow meter and temperature controller for returning the fluid to its initial condition. The test section followed a 2000 mm long (110 hydraulic diameters in length) calming section of Plexiglas to allow the hydraulically fully developed flow at the mass transfer section. The detail of the test section is shown in Fig. 1. The hydraulic diameter of the duct is 18.1 mm and the apex angle is 11.4°. All the electrodes are made of nickel. Mass transfer coefficient was measured by using ferricyanide/ferrocyanide redox reaction. The detals of the electrochemical method have been reviewed by Mizushina [7]. In this experiments, anode was located on the opposite side of cathode, and anode had an area of $100 \times 600\,mm^2$. To obtain the fully developed condition of mass transfer, the cathode had a mass transfer developing region of 275 mm (15.2 hydraulic diameter in length) as shown in Fig. 1(b). This entrance length was determined according to the experimental results of Shaw *et al.* [8] who discussed the fully developed condition of mass transfer in a round tube. Following the entrance region, an electrode with an area of $20 \times 100\,mm^2$ was set for the measurement of the overall mass transfer coefficient. Next, 20 rectangular electrodes for the local mass transfer measurements were located. Each rectangular electrode was $4 \times 60\,mm^2$ and isolated by means of epoxy resin. The same kinds of electrodes mentioned above were also located on the base wall of the isosceles triangular duct.

The point electrode (diameter 0.6 mm) was used to

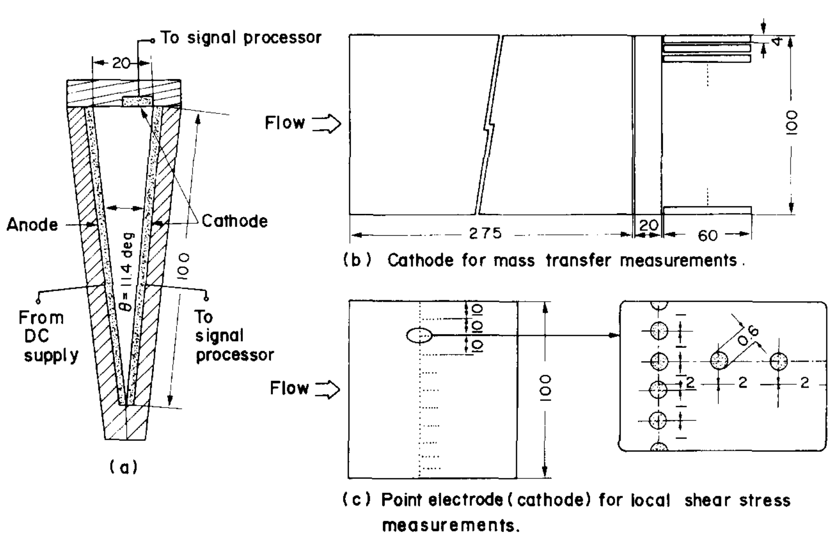

FIG. 1. Detail of the electrodes (all dimensions are in mm).

measure the time averaged and fluctuating wall shear stresses. The principle of the shear stress measurements is described in detail by Mizushina [7]. The location of the point electrode is shown in Fig. 1(c). The electrodes were separated 1 mm from each other in the lateral direction and 2 mm in the longitudinal direction. The total number of flush-mounted point electrodes in the lateral direction was 100. In the longitudinal direction, the electrodes were aligned in 10 rows, and each row had 10 electrodes, respectively. No mass transfer developing electrode was used for the measurements of shear stress and fluctuating mass transfer coefficients. Two point electrodes were selected arbitrarily, and the space correlation of the fluctuating mass transfer coefficients on these point electrodes was calculated by means of TEAC PS-80 computer system with A–D converter. The sampling frequency of A–D conversion was 200 Hz, and the data size was 8000 for each electrode.

Since it was very difficult to embed the mass transfer electrodes and the point electrodes on the same surface, two side walls, indicated in Figs. 1(b) and (c) respectively, were constructed and used separately. However, the base wall electrodes for the local and space averaged mass transfer measurements were fixed to the anode side wall for the convenient construction of a triangular duct. Thus the base wall had no point electrode.

The friction factor at the fully developed region was calculated from the pressure drop measurements. The temperature of the test liquid was controlled within 293 ± 0.1 K. The electrolyte had a composition of 0.01 M potassium ferri-ferrocyanide and 0.5 M sodium hydroxide. The density and kinematic viscosity of the test fluid were 1025 kg/m^3 and 1.077 × 10^{-4} m^2/s, respectively. The diffusion coefficient for the ferricyanide ion was 6.61 × 10^{-10} m^2/s, and the Schmidt number at the experimental condition was equal to 1630.

3. EXPERIMENTAL RESULTS AND DISCUSSION

The results of friction factor measurements were shown in Fig. 2. The friction factor of isosceles triangular ducts have been measured by [9] for the wide range of apex angles ($\theta = 4 \sim 39°$). The solid line in Fig. 2 is the empirical correlation of the friction factor given by [9] for the same geometry as the present experimental apparatus. The friction factors of this work coincide well with their data, and both results are around 15% lower than that of turbulent round tube flow. The experimental results indicated by a solid circle (●) in Fig. 2 were obtained from the integration of the local shear stress. The agreement between the shear stress and pressure drop measurements confirms, indirectly, the reliability of the electrochemical technique.

Figure 3 shows the results of overall the Sherwood number defined by $\overline{Sh} = \bar{K}\,d_h/D$, where $\bar{K}$ is the space averaged mass transfer coefficient over the whole periphery of the triangular duct. The solid lines shown in Fig. 3 are calculated for the case of $Sc = 1630$ using the previous predicting equations proposed by [10–12]. These equations are applicable to the high Schmidt number region in a turbulent pipe flow. Present experimental results are almost 35% lower than these predictions. The broken line in the same diagram was obtained assuming that Chilton–Colburn's analogy held in this system, and further assuming that the friction factor in a triangular duct was given experimentally by Fig. 2. The results of $\overline{Sh}$ are again lower than this broken line. This means that the decrease of overall mass transfer coefficient cannot be explained by the analogy between momentum and mass transfer. As stated previously, Eckert and Irvine [4] reported that overall heat transfer coefficient in a triangular duct of $\theta = 11.4°$ decreases 50% from the value of a turbulent pipe flow. They used the constant heat flux condition; the experimental condition of this work corresponds to constant wall temperature. In addition, our Schmidt number is much larger than the Prandtl number in Eckert and Irvine's experiments. Thus, it is difficult to compare our results directly with their heat transfer data. However, it is evident that both sets of results shows a more significant decrease in heat and mass transfer coefficient than that of friction factor.

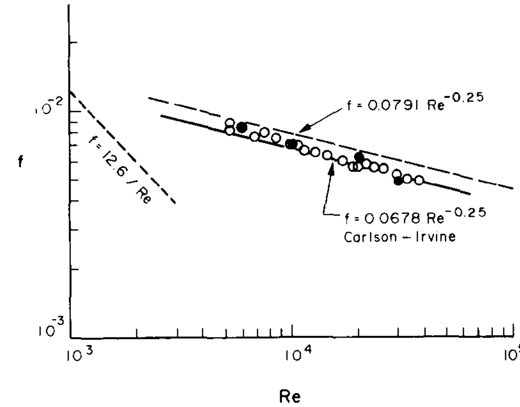

FIG. 2. Friction factor vs Reynolds number; $\theta = 11.4°$; (○) pressure drop measurements; (●), integral averaged value of local shear stress.

To discuss the anomalous decrease in overall mass transfer coefficient, the distributions of local wall shear stress and local mass transfer coefficient were measured, and are shown in Figs. 4 and 5, respectively. The local shear stress increases linearly from the apex over a considerable range of z/L ($= 0 \sim 0.7$). The experimental results do not show the strong dependence upon the Reynolds number and show a good agreement with the prediction of [6]. The distribution of the local Sherwood number shown in Fig. 5 are more gently sloping than the local shear stress distributions. Near the apex, the results at higher Reynolds number show a higher value of Sherwood number, and the opposite tendency is observed near the base of the isosceles triangle. The distribution of local Sherwood number on the base wall, indicated at $z/L = 1.0 \sim 1.1$ in Fig. 5, are nearly constant and have almost the same value as the local Sherwood number on the side wall at $z/L = 0.9 \sim 1.0$. The wall temperature distributions obtained by [4] in the heat transfer experiments of the same cross-sectional triangular duct showed the same tendency. These experimental results suggest that the flow near the base wall is approximately the same as the flow near the side wall if the distance from the base apex is the same. Thus, the integration of the local shear stress over the whole periphery was done by assuming that the shear stress distribution on the base wall was the same as that on the side wall at $z/L = 0.9 \sim 1.0$. The integrated results obtained in this way were shown in Fig. 2 and discussed previously comparing with the results of pressure drop measurements. The distributions of local Sherwood number shown in Fig. 5 were integrated and indicated in Fig. 3 by a solid circle (●). The agreement with the results of overall mass transfer electrode is good. It must be pointed out, however, that the distribution shown in Fig. 5 is greatly different from that obtained by the heat transfer experiments of [4]. The results of heat transfer experiments under the constant heat flux condition showed a more significant decrease of local heat transfer coefficient near the apex. The difference between constant heat flux and constant wall temperature (or concentration) should be examined carefully in future investigations.

The results of local shear stress and local Sherwood number measurements suggested that the turbulence structure should be changed remarkably along the side wall of the triangular duct. Thus the variation of space correlation coefficient in the lateral direction was measured using the method described in the previous section. The space correlation coefficient R_z is defined as:

$$R_z = \overline{k'(z)k'(z + \Delta z)}/\overline{[k'(z)^2]}^{1/2}\overline{[k'(z + \Delta z)^2]}^{1/2} \quad (1)$$

where k' is the fluctuating mass transfer coefficient on the point electrode. The reference position, z, is indicated by the semi-dotted line —.— in Fig. 6. The

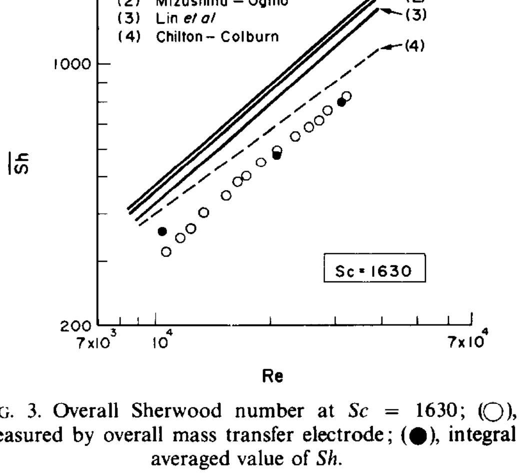

FIG. 3. Overall Sherwood number at Sc = 1630; (○), measured by overall mass transfer electrode; (●), integral averaged value of Sh.

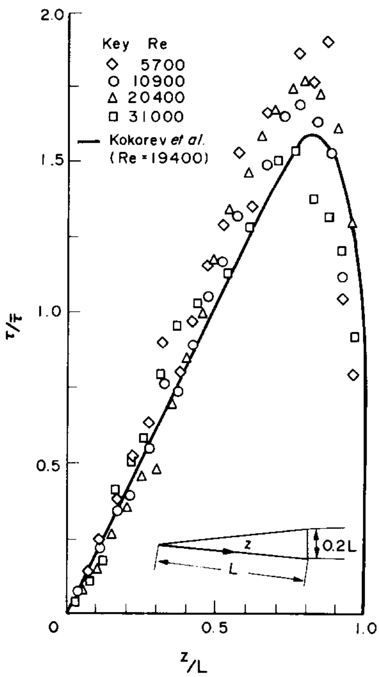

FIG. 4. Distribution of local shear stress.

distance between the two electrodes is given by Δz, one electrode being located at the reference position. The results shown in Fig. 6 are clearly subdivided into two regions. Near the apex (at $z/L < 0.2$) the space correlation coefficient is very large and this region seems to correspond to the 'laminar' region. At $z/L > 0.3$ the space correlation shows the characteristics of turbulent flow. The space correlation decreases rapidly to zero or negative value. Next, the distance Δz between the two point electrodes was non-dimensionalized by local shear velocity, u^*, which was calculated from the local shear stress shown in Fig. 4. Using the non-dimensional distance Δz^+, the results in the fully turbulent zone ($z/L > 0.3$) of Fig. 6 are replotted in Fig. 7. This diagram also contains the experimental results at Re = 10,900. Although considerable scatter of experimental data is observed, it seems that the data as a whole indicate a single profile. The solid line and the broken line are the results in a turbulent round tube flow measured by [13] and [14], respectively. The present experimental results shown almost the same profile as those obtained in a round tube. However, the integral scale obtained from the present results may be larger than that of a round tube flow. The difference in integral scale will be discussed a little later combined with results of Eulerian time correlation. At the present stage, we can say at least that the lateral space correlation coefficient in the turbulent zone is evaluated universally if the lateral distance is non-dimensionalized by local shear velocity. The longitudinal space correlation was also measured by means of the same technique. However, since only the small misalignment in the longitudinal direction caused a superimposition of the lateral space

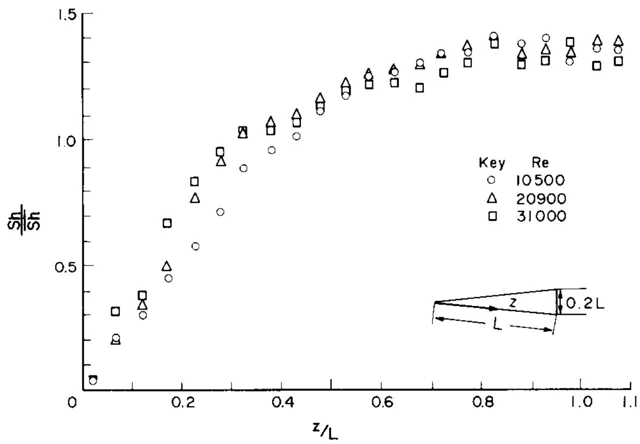

FIG. 5. Distribution of Sh (data at $z/L = 1.0 \sim 1.1$ correspond to the results on the base wall).

correlation on the longitudinal one, it was impossible to obtain quantitative results of the longitudinal space correlation coefficient.

If the velocity profile in the concentration boundary layer is assumed to be linear, the fluctuating velocity near the wall, u', can be related to the fluctuating velocity gradient, s'_x, by

$$\lim_{y \to 0} u'/\bar{u} = s'_x/\bar{s}_x \quad (2)$$

where $\bar{u}$ and $\bar{s}_x$ are the local time averaged velocity and velocity gradient, respectively. Combining the above relationship with the pseudo-steady solution of the time dependent concentration boundary layer equation, turbulent intensity on the wall is calculated by [7] to be

$$\lim_{y \to 0} \frac{\overline{(u'^2)}^{1/2}}{\bar{u}} = 3\frac{\overline{(k'^2)}^{1/2}}{\bar{k}}. \quad (3)$$

If more precise analysis is desired, a capacitance effect caused by the time delay in the mass transfer response to the fluctuation of velocity field must be taken into account as pointed out by [14]. Because of the smallness of the point electrode, however, the error caused by the neglect of the capacitance effect was estimated as less than 5% from the mass transfer spectrum at Re = 31,000 and z/L = 0.7 where the fluctuation of velocity field was expected to be most violent in these experiments. In addition, this correction unavoidably contained the error caused by the noise of the data acquisition system. The noise level recorded on the magnetic tape without the mass transfer signal was 3.5% of the intensity in the mass transfer fluctuation with the same experimental condition mentioned above. Thus the capacitance effect was neglected in this study.

As shown in Fig. 7, the lateral turbulence scale on the side wall is quite small. Besides, the point electrode has a finite size (0.6 mm dia.). This emits the non-

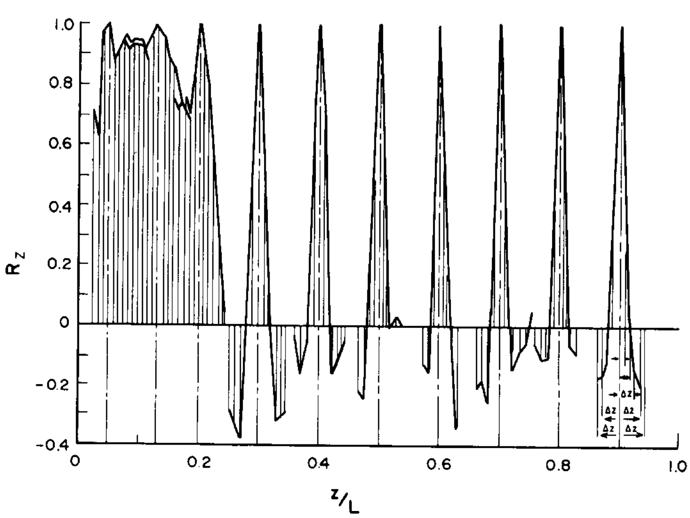

FIG. 6. Lateral space correlation coefficient along the side wall at Re = 5700. The reference position, z, is indicated by ——.——, and Δz is typically shown at z/L = 0.9.

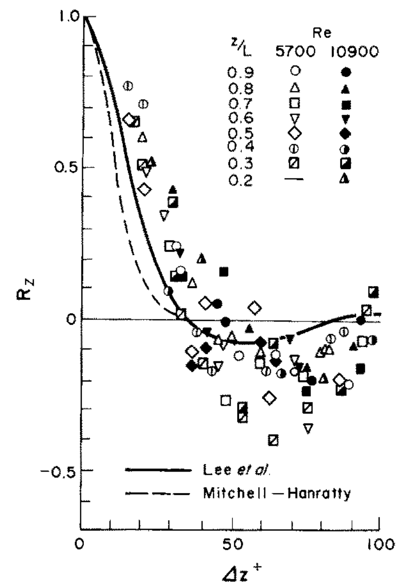

FIG. 7. Non-dimensionalized representation of the lateral space correlation coefficient.

uniform flow over the electrode in the lateral direction. For example, the non-dimensional radius a^+ $(=au^*/\nu)$ of a point electrode at $Re = 31{,}000$ and $z/L = 0.7$ was 30.9, while at a lower Reynolds number (Re = 5700), the same point electrode has a radius of $a^+ = 8.2$. Thus, in comparison with the results in Fig. 7, it is evident that a correction of non-uniform flow over the electrode is necessary. The following correction equation proposed by [15] was used:

$$\frac{\overline{k_0'^2}}{\overline{k'^2}} = \frac{\pi^2 a^4}{4} \int_{-a}^{+a} \int_{-a}^{+a} [(a^2 - z_i^2) \times (a^2 - z_j^2)]^{1/2} R_z \, dz_i dz_j \quad (4)$$

where $\overline{k_0'^2}$ is the measured intensity of mass transfer fluctuation, R_z is the lateral space correlation coefficient and Δz in equation (1) should be replaced by $|z_i - z_j|$. The integral scale of this experiment was determined as $\Lambda^+ = 21.0$ from Fig. 7, and the space correlation in the lateral direction was approximated as

$$R_z = \exp(-|z_i^+ - z_j^+|/21.0). \quad (5)$$

Assuming the space correlation shown in Fig. 7 to be independent of Reynolds number, this equation was used for the correction of non-uniform flow even at higher Reynolds number. The typical values of the correction factor at z/L = 0.5 were 1.435; 1.656; 2.17 and 2.85 at Re = 5700; 10,900; 20,400 and 31,000, respectively.

The distribution of turbulent intensity on the wall calculated from equations (3)–(5) is shown in Fig. 8. In the fully turbulent region near the base, the turbulent intensity is almost constant $[(\overline{u'^2})^{1/2}/\bar{u} = 0.21]$. This value is compared in Fig. 9 with the previous works in turbulent boundary layer or turbulent round tube flows. Eckerman [16], Zaric [17] and Ueda and Hinze [18] measured the turbulent intensity by means of a hot wire anemometer. Although the present results show a good agreement with the extrapolated values of these hot wire measurements, the simple extrapolation may be unprovable. In fact, Mitchell and Hanratty [14] employed the same technique as this work, and determined the turbulent intensity on the wall as $(\overline{u'^2})^{1/2}/\bar{u} = 0.32$ for turbulent tube flow. Since the results of [14] are widely accepted, the present data at the turbulent zone are regarded as the results of considerable damping of turbulence near the wall judging by the results of a round tube flow. Approaching the apex, the distribution of turbulent intensity in Fig. 8 shows a strong dependence upon Reynolds number. At Re = 31,000, the intensity seems to be damped in the region of $0 < z/L < 0.2$. At the lowest Reynolds number (Re = 5700), the turbulent intensity begins to decrease at z/L = 0.5, and seems to be

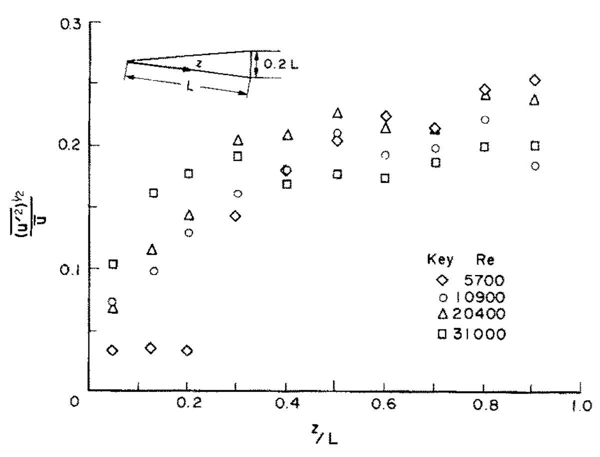

FIG. 8. Distribution of turbulent intensity on the side wall.

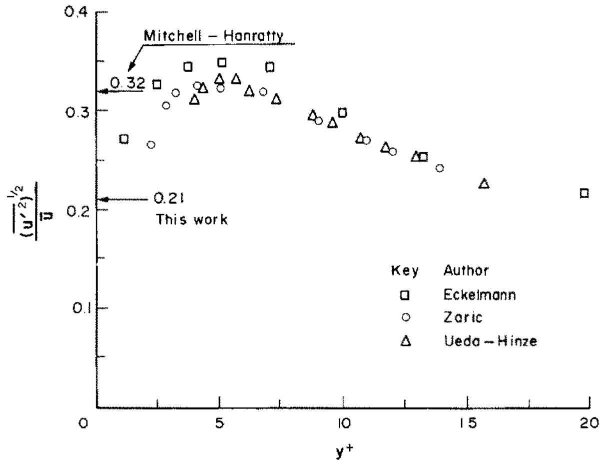

FIG. 9. Comparison of turbulent intensity near the wall.

completely damped at $z/L = 0\sim0.2$. This region corresponds to the 'laminar region'. The transitional region seems to exist between the 'laminar region' and the fully turbulent region. This considerably wide transitional region is expected to play a significant role in the decrease of the overall mass transfer coefficient.

Although it was impossible to measure quantitatively the space correlation in the longitudinal direction because of the misalignment of point electrodes, the convective velocity, U_c, of the large eddy near the wall can be determined precisely from the space and time correlation in the longitudinal direction defined by

$$R_{x,t} = \overline{k'(x,\,t)\,k'(x + \Delta x,\,t + \Delta t)}/(\overline{k'(x)^2})^{1/2}\,(\overline{k'(x + \Delta x)^2})^{1/2}. \quad (6)$$

In this experiment, Δx was fixed at 8 or 10 mm, and the delay time, Δt, was determined so that $R_{x,t}$ had a maximum value. The convective velocity is given by $U_c = \Delta x/\Delta t$. The distribution of U_c is shown in Fig. 10. This diagram indicates that a convective velocity near the base is alomost equal to the averaged velocity. Approaching to the apex, the convective velocity decreases gradually. However, this velocity does not become zero even very near the apex. Although the dependence of the convective velocity distribution upon Reynolds number could exist, the scatter of experimental data shown in Fig. 10 prevents us reaching any conclusion about the Reynolds number dependence.

Eulerian time correlation of the fluctuating mass transfer coefficient on a point electrode is defined as

$$R_t = \overline{k'(t)k'(t + \Delta t)}/\overline{k'^2} \quad (7)$$

where Δt is the delay time. Assuming that the representative velocity near the wall was equal to the convective velocity defined above, the delay time was non-dimensionalized as $\Delta t\ U_c\ u^*/v$ which may correspond to the non-dimensional distance, Δx^+, in the longitudinal direction. The distribution of R_t at Re = 31,000 is shown in Fig. 11, indicating that the univer-

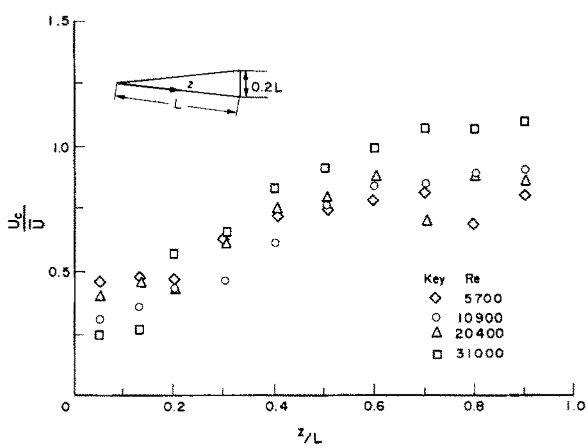

FIG. 10. Distribution of the convective velocity.

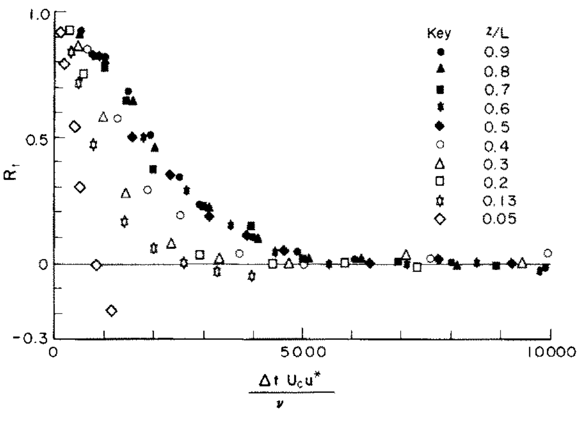

FIG. 11. Dependence of Eulerian time correlation coefficient upon the distance from the apex at $Re = 31{,}000$.

sal distribution is obtainable at $z/L = 0.5 \sim 1.0$. This region should be considered as a fully turbulent zone, and is considerably narrower than the constant turbulent intensity region shown in Fig. 8. The same tendency was observed at the different Reynolds number, although the results are not presented here. The integral scale, τ_E, of Eulerian time correlation at the fully turbulent region (at $z/L = 0.5 \sim 1.0$) is shown in Fig. 12 together with the lateral integral scale, Λ_z, of the space correlation which was shown in Fig. 7. The longitudinal integral scale is much larger than the lateral integral scale, i.e. $\tau_E \bar{U}_c/\Lambda_z \simeq 40 \sim 50$. The longitudinal integral scale seems to depend more significantly upon Reynolds number. The integral scales in a turbulent tube flow obtained by the previous investigators [13, 14, 19] are also shown in Fig. 12. The present results are almost two or three times larger than those in a round tube flow. In addition, the decrease of turbulent intensity near the wall have already been observed in Fig. 9. Although measurements of secondary flow were

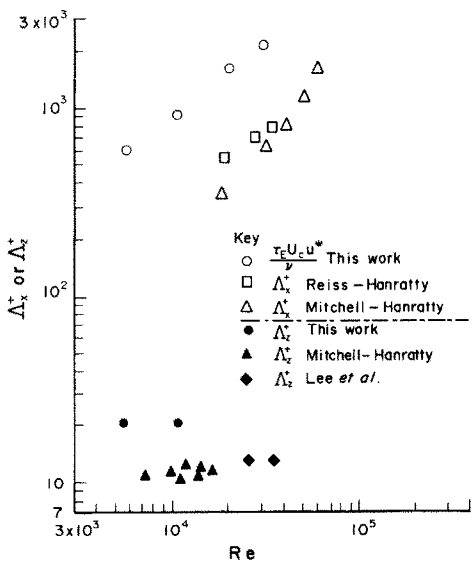

FIG. 12. Integral scales in the longitudinal and lateral directions.

not made in this study, the effect of the secondary flow may play a significant role in the turbulent triangular duct flow. The decrease in turbulent intensity or the increase in integral scales observed in this work are possibly affected by the secondary flow. However the interaction between the change of turbulence structure and secondary flow is not well understood at the present stage. More precise measurements of turbulent characteristics containing the secondary flow is expected in the future investigation to explain the decrease of the mass or heat transfer coefficient in a triangular duct flow.

In the previous discussion, the 'fully turbulent' region was defined rather arbitrarily for the convenience of each discussion of experimental results. Three definitions were employed in this work. In Fig. 6, the fully turbulent region was defined as a region where the lateral space correlation showed a turbulent characteristic. Next, the constant turbulent intensity region on the side wall was also defined as the fully turbulent region (see Fig. 8). The third definition of the fully turbulent region was given as the universal distribution region of Eulerian time correlation shown in Fig. 11. The determination of 'laminar' and 'turbulent' regions using above-mentioned definitions is shown in Fig. 13. This diagram contains also the experimental results of [1]; the criterion for the lateral space correlation of this work is in good agreement with their velocity distribution measurements. The complete laminar region should correspond to the region under the solid line in Fig. 13 which was determined by flow instability visualization. Above this solid line, the flow condition may be fully turbulent or transitional. Many kinds of definition for the fully turbulent region are possible, and each definition gives a different criterion of turbulent region as shown in Fig. 13. At present, it is hard to say which definition is most reasonable. However, it should be pointed out that the transitional region, the region between the solid line and each broken line in Fig. 13, is considerably wide irrespective of the definition of the fully turbulent region.

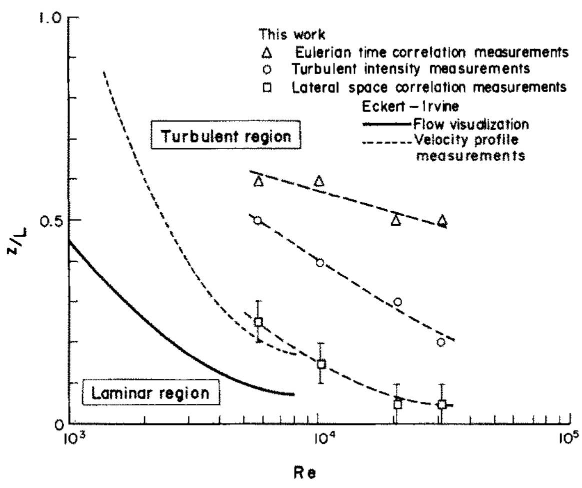

FIG. 13. Determination of laminar and turbulent regions by various kinds of definitions.

4. CONCLUSION

The electrochemical method applied to a triangular flow has revealed some turbulent characteristics in a non-circular duct. Turbulent intensity and space correlation on the side wall are remarkably changed because of the side wall effect near the apex. In addition, even in the fully turbulent region near the base of a triangle, turbulent intensity and space correlation are different from those in a turbulent round tube flow. The damp of the turbulent intensity and the increase of turbulent scales near the wall over the whole side wall seem to correspond to the decrease in the overall or local mass transfer coefficient of an Isosceles triangular duct flow with a narrow apex angle.

Acknowledgment—The authors gratefully acknowledge the invaluable discussions provided by Prof. T. F. Irvine, Jr. in State University of New York at Stony Brook during the course of this work. The authors acknowledge also the assistance of Mr. Y. Sato and H. Tamagi in making many of the measurements. This work was partially supported by the Saneyoshi Scientific Technology Fundation.

REFERENCES

1. E. R. G. Eckert and T. F. Irvine, Jr., Flow in corners of passages with noncircular cross section, *Trans. A.S.M.E.* **78**, 709–718 (1956).
2. R. W. Hanks and J. C. Brooks, Birefringent flow visualization of transitional flow phenomena in an isosceles triangular duct, *AIChE Jl* **16**, 483–489 (1970).
3. P. C. Bandopadhayay and J. B. Hinwood, On the coexistence of laminar and turbulent flow in a narrow triangular duct, *J. Fluid Mech.* **59**, 775–784 (1973).
4. E. R. G. Eckert and T. F. Irvine, Jr., Pressure drop and heat transfer in a duct with triangular cross section, *J. Heat Transfer* **82**, 125–138 (1960).
5. R. G. Deissler and M. F. Taylor, Analysis of turbulent flow and heat transfer in noncircular passages, NACA TN 4384 (1958).
6. L. S. Kokorev, A. S. Korsun, B. N. Kostyunin and V. I. Petrovichev, Hydraulic drag and heat transfer in turbulent flow of liquids in triangular channels, *Heat Transfer Sov. Res.* **3**, 56–65 (1971).
7. T. Mizushina, The electrochemical method in transport phenomena, in *Advances in Heat Transfer* (Edited by J. P. Hartnett and T. F. Irvine, Jr.), Vol. 7, p. 87. Academic Press, New York (1971).
8. P. V. Shaw, L. P. Reiss and T. J. Hanratty, Rates of turbulent transfer to a pipe wall in the mass transfer entry region, *AIChE Jl* **9**, 362–364 (1963).
9. L. W. Carlson and T. F. Irvine, Jr., Fully developed pressure drop in triangular shaped ducts, ASME Paper No. 60-WA-100 (1963).
10. T. S. Son and T. J. Hanratty, Limiting relation for the eddy diffusivity close to a wall, *AIChE Jl.* **13**, 689–696 (1967).
11. T. Mizushina and F. Ogino, Eddy viscosity and universal velocity profile in turbulent flow in a straight pipe, *J. chem. Engng. Japan* **3**, 166–170 (1970).
12. C. S. Lin, R. W. Moulton and G. L. Putnum, Mass transfer between solid wall and fluid streams, *Ind. Engng Chem.* **45**, 636–646 (1953).
13. M. K. Lee, L. D. Eckelman and T. J. Hanratty, Identification of turbulent wall eddies through the phase relation of the components of the fluctuating velocity gradient, *J. Fluid Mech.* **66**, 17–33 (1974).
14. J. E. Mitchell and T. J. Hanratty, A study of turbulence at a wall using an electrochemical wall shear-stress meter, *J. Fluid Mech.* **26**, 199–221 (1966).
15. P. V. Shaw and T. J. Hanratty, Fluctuations in the local rate of turbulent mass transfer to a pipe wall, *AIChE Jl.* **10**, 475–482 (1964).
16. H. Eckelman, An experimental investigation of a turbulent channel flow with a thick viscous sublayer, *Max-Plank-Institut, Göttingen*, No. 101 (1973).
17. Z. Zaric, *Turbulent Forced Convection in Channels and Bundles* (Edited by S. Kacak and D. B. Spalding), Vol. 1, p. 377. Hemisphere, Washington (1979).
18. H. Ueda and J. O. Hinze, Fine structure turbulence in the wall region of a turbulent boundary layer, *J. Fluid Mech.* **67**, 125–143 (1975).
19. L. P. Reiss and T. J. Hanratty, An experimental study of the unsteady nature of the viscous sublayer, *AIChE Jl.* **9**, 154–160 (1963).

MESURES DE TURBULENCE ET DE TRANSFERT MASSIQUE DANS UN ECOULEMENT ETABLI DANS UN CANAL A SECTION TRIANGULAIRE AVEC UN PETIT ANGLE AU SOMMET

Résumé—Une méthode électrochimique est appliquée aux mesures de transfert massique dans un écoulement turbulent établi dans un canal à section en triangle isocéle avec une petit angle au sommet. L'analyse du coefficient de transfert fluctuant mesuré sur une électrode ponctuelle porte sur la distribution de l'intensité de turbulence et le coefficient de corrélation spatiale sur la paroi. Dans la région laminaire ou de transition près du sommet, un changement remarquable est détecté dans l'intensité de turbulence et dans la corrélation spatiale. De plus, les caractéristiques turbulentes au voisinage de la base changent considérablement par rapport à celles relatives à l'écoulement turbulent dans une section circulaire pour le même nombre de Reynolds. Le décroissement du coefficient de transfert massique moyen dans un conduit triangulaire est qualitativement expliqué par le changement de structure de la turbulence de paroi.

MESSUNGEN DES TURBULENZGRADES UND DES STOFFTRANSPORTS BEI VOLLAUSGEBILDETER STRÖMUNG IN EINEM KANAL DREIECKIGEN QUERSCHNITTS MIT SPITZEM SCHEITELWINKEL

Zusammenfassung—Die elektrochemische Methode wurde zur Messung des Stofftransports bei vollausgebildeter Strömung in einem Kanal dreieckigen Querschnitts mit spitzem Scheitelwinkel angewandt. Die Analyse der an einer punktförmigen Elektrode gemessenen Schwankungen des Stofftransportkoeffizienten ergab die Turbulenzverteilung und den Korrelations-Koeffizienten an den Seiten des Dreiecksquerschnitts. Im laminaren sowie im Übergangsgebiet ist in der Nähe des Scheitels eine bemerkenswerte Änderung des Turbulenzgrades und des Korrelations-Koeffizienten festzustellen. Außerdem ist selbst im vollkommen turbulenten Bereich in der Nähe der Dreiecksbasis die Turbulenzcharakteristik ganz nah an den Seitenwänden sehr verschieden von derjenigen einer turbulenten Kreisrohrströmung bei derselben Reynolds Zahl. Die Abnahme des Gesamtstofftransport-Koeffizienten in einem dreieckigen Kanalquerschnitt wird qualitativ durch die veränderte Turbulenzstruktur an den Wänden gedeutet.

ИССЛЕДОВАНИЕ ТУРБУЛЕНТНОСТИ И МАССОПЕРЕНОСА ПРИ ПОЛНОСТЬЮ РАЗВИТОМ ТЕЧЕНИИ В ТРУБЕ С СЕЧЕНИЕМ В ФОРМЕ РАВНОБЕДРЕННОГО ТРЕУГОЛЬНИКА С ОСТРЫМ УГЛОМ У ВЕРШИНЫ

Аннотация — Электрохимическим методом исследуется массоперенос при полностью развитом турбулентном течении в трубе с сечением в форме равнобедренного треугольника с острым углом у вершины. В результате анализа пульсационных значений коэффициента массопереноса, измеренных точечным электродом, получены распределения интенсивности турбулентности и коэффициент пространственной корреляции на боковой стенке треугольника. В ламинарной или переходной области у вершины треугольника происходит существенное изменение интенсивности турбулентности и пространственной корреляции. Кроме того, даже в полностью турбулентной области у основания трегольника характеристики турбулентности у боковых стенок значительно отличаются от величин, характерных для турбулентного течения в круглой трубе при том же значении числа Рейнольдса. Дано качественное объяснение влияния структуры пристенной турбулентности на уменьшение суммарного коэффициента массопереноса в трубе треугольного профиля.